6156–6165 *Nucleic Acids Research, 2015, Vol. 43, No. 12* *Published online 27 May 2015*
doi: 10.1093/nar/gkv570

Multivalent ion-mediated nucleic acid helix-helix interactions: RNA versus DNA

Yuan-Yan Wu[1], Zhong-Liang Zhang[1], Jin-Si Zhang[1], Xiao-Long Zhu[2] and Zhi-Jie Tan[1,*]

[1]Department of Physics and Key Laboratory of Artificial Micro & Nano-structures of Ministry of Education, School of Physics and Technology, Wuhan University, Wuhan 430072, China and [2]Department of Physics, School of Physics & Information Engineering, Jianghan University, Wuhan 430056, China

Received March 22, 2015; Revised May 19, 2015; Accepted May 20, 2015

ABSTRACT

Ion-mediated interaction is critical to the structure and stability of nucleic acids. Recent experiments suggest that the multivalent ion-induced aggregation of double-stranded (ds) RNAs and DNAs may strongly depend on the topological nature of helices, while there is still lack of an understanding on the relevant ion-mediated interactions at atomistic level. In this work, we have directly calculated the potentials of mean force (PMF) between two dsRNAs and between two dsDNAs in $Co(NH_3)_6^{3+}$ (Co-Hex) solutions by the atomistic molecular dynamics simulations. Our calculations show that at low [Co-Hex], the PMFs between B-DNAs and between A-RNAs are both (strongly) repulsive. However, at high [Co-Hex], the PMF between B-DNAs is strongly attractive, while those between A-RNAs and between A-DNAs are still (weakly) repulsive. The microscopic analyses show that for A-form helices, Co-Hex would become 'internal binding' into the deep major groove and consequently cannot form the evident ion-bridge between adjacent helices, while for B-form helices without deep grooves, Co-Hex would exhibit 'external binding' to strongly bridge adjacent helices. In addition, our further calculations show that, the PMF between A-RNAs could become strongly attractive either at very high [Co-Hex] or when the bottom of deep major groove is fixed with a layer of water.

INTRODUCTION

Nucleic acids are highly charged polyanions (1). The structural folding of nucleic acids into compact native structure generally experiences strong Coulomb repulsive force, while metal ions in solution would bind to nucleic acid surface to reduce the Coulomb repulsion during folding (2–11). Therefore, metal ions play a critical role in the folding thermodynamics and kinetics of nucleic acids (2–11).

The double-stranded (ds) helix is a fundamental segment in nucleic acid structures (1). The ion-mediated interaction between two ds helices would provide the energetics for RNA structural collapse and DNA condensation (1–11). For dsDNAs, the existing experiments suggest that monovalent ions can only mediate an inter-helix repulsion, while multivalent ions can induce an attractive force and consequently cause DNA condensation (2,4–6,12–19). Such multivalent ion-mediated effective attraction has also been proposed to cause the condensation of other like-charged polyelectrolytes (20–25).

Due to the similarity between dsDNA and dsRNA in charge density (1), it is natural to assume that the ion-mediated force between dsRNAs would be similar to that between dsDNAs, and short dsDNAs have been used instead of dsRNAs to probe the ion-dependent structural assembly of nucleic acid helices (26–29) despite their different helix structures. However, the recent UV adsorption experiments have shown that in 20 mM Na^+ buffer, ∼4 mM Cobalt hexamine ($Co(NH_3)_6^{3+}$, i.e. Co-Hex) ions can cause the aggregation of short dsDNAs, but cannot lead to the aggregation of short dsRNAs (30,31). The remarkable finding is beyond the expectation and has been proposed to be attributed to the binding of Co-Hex ions into deep major groove of RNAs (30–32). However, there is still lack of a direct illustration on the linkage between ion-mediated interaction and the relevant ion-binding structure, corresponding to the experimental ionic conditions (30–32). In this work, we will directly calculate the potentials of mean force between two dsRNAs as well as those between two dsDNAs, in order to directly establish the relationship between the ion-mediated effective force and the ion-binding structures.

Several polyelectrolyte theories have been developed and employed to predict the ion-mediated interaction between like-charged polyelectrolytes. The counterion condensation theory has been developed based on line-charge structural model of infinite length, while the theory always predicts effective attractive forces between dsDNAs even at low monovalent salt and is only applicable to line-charge polyelectrolytes (33,34). The Poisson-Boltzmann theory with mean-

*To whom correspondence should be addressed. Tel: +86 27 68752989 3225; Fax: +86 27 68752569; Email: zjtan@whu.edu.cn

field assumption ignores the ion-ion correlations and thus always predicts effective repulsive force between dsDNAs even at high multivalent salt (35–41). The electrostatic zipper model can predict an effective force between two helices at multivalent salt while the partition of binding ions into major/minor grooves is somewhat *ad hoc* (42,43). The tightly bound ion model which accounts for ion-ion correlation can predict the ion-mediated effective force between dsDNAs, while the model assumes the distribution of molecular charges on phosphate groups and thus may not make reliable predictions on ion-binding structures near helix grooves (44–47). Therefore, the existing theories could not give an *ab initio* and direct illustration on the multivalent ion-mediated effective interaction between dsRNAs (and dsDNAs) and the microscopic ion-binding structure. As an important bridge between experiments and theories, the computer simulations can be a powerful tool to probe the effective interactions between biomolecules (48–57). Beyond the simplified Monte Carlo and Langevin dynamics simulations (e.g. 47–50), the all-atomistic molecular dynamics (MD) explicitly takes into account the detailed atomistic structure of nucleic acids, ions, and water molecules, and thus could give a direct and detailed exploration on the effective interactions between biomolecules (48–63).

In this study, we will employ the all-atomistic MD simulations to directly calculate the potentials of mean force (PMF) between A-form RNAs (A-RNAs) and those between B-form DNAs (B-DNAs) in Co-Hex salt solutions. We will also make further calculations for A-form DNAs (A-DNAs) and for the A-RNAs with the spatial ion-accessible region modified. Correspondingly, the detailed Co-Hex binding structures will be analyzed. We will also make the direct comparisons with the related experiments. The present work would give atomistic level calculations on the effective interactions between dsRNAs as well as those between dsDNAs, and would present a direct illustration on the relationship between ion-mediated effective interactions and ion-binding structures.

MATERIALS AND METHODS

All-atomistic molecular dynamics simulations

In the work, we will calculate the PMFs between two A-RNAs, between two B-DNAs and between two A-DNAs by the atomistic MD simulations. The A-RNA, B-DNA and A-DNA helices are of 16-bp length, and their atomic structures are displayed in Figure 1. The sequences of the helices are selected according to the recent experiments (30–32) and contain all the dinucleotide base pairs; see Supplementary Table S1 in Supplementary Material.

The structures of the 16-bp nucleic acid helices are taken as the standard A-RNA, B-DNA and A-DNA fibers. The two parallel A-RNA (or DNA) helices with axes in z direction are separated in x direction and immersed in a rectangle box containing explicit water and ions. The A-RNAs (or DNAs) are harmonically restrained with 1000 kJ/(mol·nm^2) force constant in y and z directions, thus are only allowed to move translationally in x direction. The size of the rectangle box is taken as $130 \times 80 \times 100$ Å^3. The Na^+ and $Co(NH_3)_6^{3+}$ (Co-Hex) ions are added with Amber tleap Program (64,65). To get the desirable bulk ion concentrations, the simplified Monte Carlo simulations (50,66) are employed to estimate numbers of Co-Hex and Na^+ ions in the simulational cell before the all-atomistic MD simulations; see Supplementary Material for details. Afterward, the numbers of Co-Hex and Na^+ ions from the simplified Monte Carlo simulations are used in the all-atomistic simulations, and the realistic bulk Na^+ and Co-Hex concentrations from the all-atomistic MD simulations are close to the desirable values; see Supplementary Figure S1 in Supplementary Material for the cases of 100 mM Na^+ and 5 mM Co-Hex solutions.

In the simulations, we employ the Amber parmbsc0 force field and the TIP3P water model combined with parmbsc0 ion model (64,65). Corresponding to the recent experiments (30–32), the solutions always contain ∼100 mM NaCl as the background, and [Co-Hex] is taken as low (0.5 mM), high (5 mM) and very high (50 mM) values, respectively. Since previous experiments showed that the octahedral coordination shell remains intact in binding to DNA (67), the Co-Hex ions are built with the explicit bonds between cobalt and amine groups and the explicit N–Co–N angles specified to generate an octahedral Co-Hex complex (68,69). The charges on a Co-Hex complex are generated based on the electrostatic potential generated with the DGAUSS program (68), and the hydrogen bonds of Co-Hex are considered with van der Waals potential with the new charge model and improved van der Waals parameters (68,70). All the parameters for Co-Hex ions are taken from (68). All the systems are optimized, thermalized (298K) and equilibrated by the program Gromacs 4.5 (71) with the periodic boundary conditions and Particle Mesh Ewald method employed (72), and a time step of 1–2 fs is used in the conjunction with LINCS algorithm (73). Firstly, an energy minimization of 5000 steps is performed with the steepest descent algorithm at low temperature, and then the systems are slowly heated to 298 K and equilibrated with the Nose–Hoover temperature coupling until 0.5 ns (74). Afterward, the subsequent NPT simulations of 2 ns (time-step 1 fs, $P = 1$ atm) are performed with the Parrinello-Rahman pressure coupling and with the nucleic acids fixed (65). Finally, each MD simulation is continued for another 60 ns in the isothermic-isobaric ensemble (time-step 2 fs, $P = 1$ atm, $T = 298$ K). Our MD simulations generally reach the equilibrium after ∼10 ns, as shown in Supplementary Figures S2 and S3 for ion-binding number and Supplementary Figures S4 and S5 for helix-helix separation versus MD time in Supplementary Material. The trajectories in equilibrium are used to calculate the PMF between two helices.

Calculating potential of mean force between two helices

In the work, we employ the pseudo-spring method (53,54,66) to calculate the PMF between two A-RNAs (or DNAs). In the method, a pseudo-spring with spring constant k is added to link the center of mass of two helices in MD simulations, as shown in Figure 1. Based on the MD trajectories in equilibrium, the effective force between the two A-RNA (or DNA) helices can be calculated by

$$F = k\Delta x, \tag{1}$$

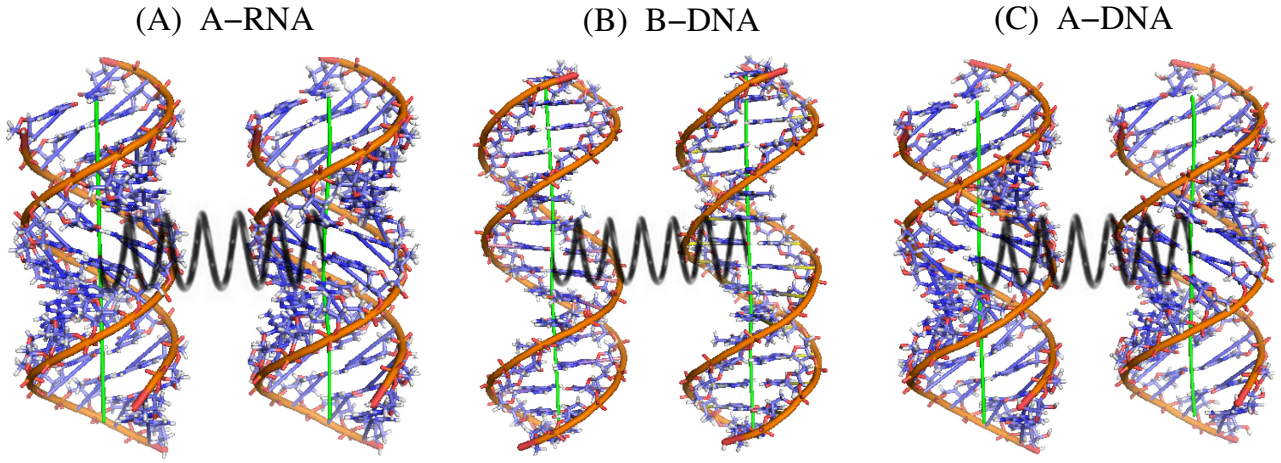

Figure 1. An illustration for two parallel 16-bp A-RNAs (**A**), B-DNAs (**B**) and A-DNAs (**C**). The spring with a spring constant k which connects the centers of mass of two helices has been used to calculate the potential of mean force between two double-stranded RNAs and DNAs (53,54,73).

where Δx is the deviation of the spring length away from the original length x_0 in equilibrium. The negative and positive Δx's correspond to the attractive and repulsive forces, respectively. After a series of $F(x)$ at different separations x are obtained, the PMF $\Delta G(x)$ between the two A-RNA (or DNA) helices can be calculated through the integration (53,54,66)

$$\Delta G(x) = G(x) - G(x_{\text{ref}}) = \int_{x}^{x_{\text{ref}}} F(x')dx', \qquad (2)$$

where x_{ref} is the outer reference separation. It has been shown previously that the pseudo-spring method is efficient and convenient in calculating PMF between two DNAs and two like-charged nanoparticles (53,54,66). In practice, the spring constant k is generally taken as 1000 kJ/(mol·nm^2) and x_{ref} is taken as 40 Å. For the cases that two helices interact very strongly, we also use a higher value of $k = 2000$ kJ/(mol·nm^2). Additionally, we have also made the additional calculations for the PMFs with the umbrella sampling method (70,71,75), and the results are very close to those from the pseudo-spring method; see Supplementary Figure S6 in Supplementary Material.

RESULTS AND DISCUSSION

In the work, we will calculate the PMF $\Delta G(x)$ between two nucleic acid helices in Co-Hex solutions by the all-atomistic MD simulations, and will examine how Co-Hex ions modulate the PMFs between dsDNAs and dsRNAs. We would emphasize illustrating the microscopic mechanism for the difference in PMFs between A-RNAs and B-DNAs.

PMFs between B-DNAs at low and high [Co-Hex]s

As shown in Figure 2a, the PMF between two B-DNAs is repulsive at low (∼0.5 mM) [Co-Hex], while becomes strongly attractive with the free energy minimum of $\sim -3.5 k_B T$ at the axis-axis separation of ∼27 Å when [Co-Hex] is increased to ∼5 mM. Such ion-mediated PMF is generally coupled to ion-binding (45,76). Due to the high entropy penalty for Co-Hex binding at low [Co-Hex], the system at low [Co-Hex] is dominated by Na^+-binding from the background of 100 mM Na^+ and the monovalent ions can only modulate repulsive PMF. In contrast, at high [Co-Hex], Co-Hex-binding would dominate the system due to lower entropy ion-binding penalty, and strong Coulomb attraction between Co-Hex and two adjacent B-DNAs could cause an attractive force. The predicted PMFs between B-DNAs are in accordance with the previous experiments which show that high [Co-Hex] could induce DNA aggregation while DNAs resist condensation at low [Co-Hex] (12–17,30,31). The axis-axis separation of ∼27 Å at the lowest ΔG(x) for ∼5 mM [Co-Hex] also agrees well with the values of equilibrium spacing of DNA aggregates from various experiments (15–19,77). In addition, following (46,78), we have calculated the osmotic pressures for hexagonal DNA aggregate, with assuming the additivity for the pair-wise PMF (28). The calculated osmotic pressures are very close to the corresponding experimental data (15,16); see Supplementary Figure S8 and Supplementary Material for details.

To gain a deep understanding on the relationship between [Co-Hex] and the PMF between B-DNAs, we would analyze the radial Co-Hex concentration distributions $c(r)$'s around B-DNAs at different [Co-Hex]'s, and $c(r)$'s have been calculated according to Eq. 9 in Ref (79). As shown in Figure 2b, Co-Hex ions would begin to bind to a B-DNA at axial distance >∼5 Å, and prefer to accumulate at the outer surface of B-DNA with the axial distance of ∼13 Å. Such binding near the outer surface of a helix with the radial distance range of [11–15 Å] will be termed as 'external binding' (31). Higher (∼5 mM) [Co-Hex] causes much more Co-Hex ions 'external binding' around B-DNAs near the radial distance of ∼13 Å than low (∼0.5 mM) [Co-Hex]. The further detailed analyses show that at low [Co-Hex], Co-Hex ions prefer to bind over the minor groove rather than the major groove, while at high [Co-Hex], Co-Hex ions mainly bind over the major groove rather than the minor groove; see Figure 2c. This is reasonable since the minor groove of B-DNA is narrower and electrically more negative, thus Co-Hex ions prefer to binding to minor groove at low [Co-Hex]

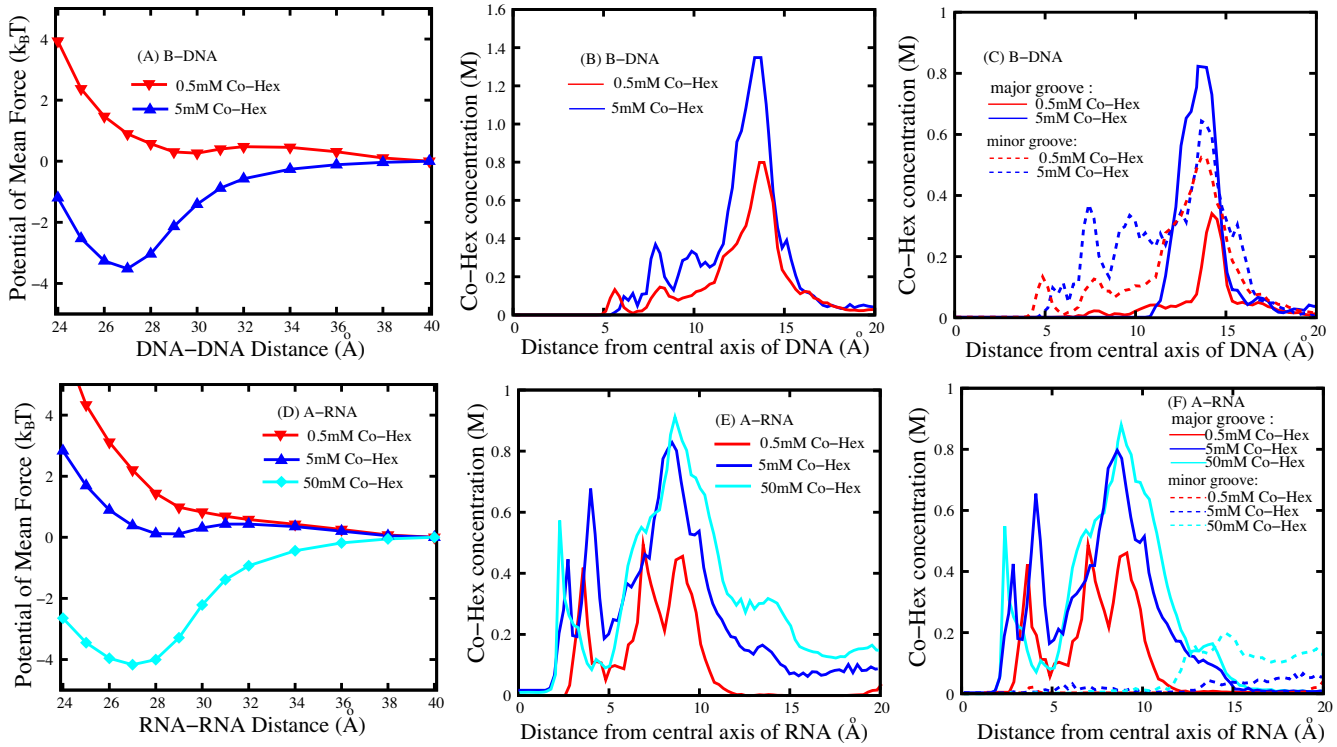

Figure 2. (**A**) The potentials of mean force between two 16-bp B-DNAs in 0.5 mM and 5 mM Co-Hex solutions. (**B**) The Co-Hex ion distributions around the B-DNA corresponding to panel a. (**C**) The Co-Hex ion distributions around B-DNA in (or over) major groove and minor groove according to panels a and b. (**D**) The potentials of mean force between two 16-bp A-RNAs in 0.5 mM, 5 mM and 50 mM Co-Hex solutions. (**E**) The Co-Hex distributions around the A-RNA corresponding to panel d. (**F**) The Co-Hex distributions around A-RNA in (or over) major groove and minor groove corresponding to panels d and e. Note that the buffers always contain 100 mM NaCl.

(31). When [Co-Hex] is increased to a high value, more Co-Hex ions become binding while the narrow minor groove has already accommodated many binding ions, causing the binding of excess Co-Hex ions over the major groove. The strong 'external binding' of Co-Hex would be shared by adjacent B-DNAs, and could cause an significantly attractive PMF between B-DNAs at high [Co-Hex] (46,53,55,66,80).

To analyze the 3-dimensional Co-Hex binding around two B-DNAs, we would illustrate the binding structure of Co-Hex ions of high concentration (74). As shown in Figure 3a and b, Co-Hex ions form the obvious ion-bridge configuration between adjacent B-DNAs which appears much more pronounced for high [Co-Hex]. Such apparent ion-bridge configuration between two helices would provide a key contribution to the attractive PMF between B-DNAs (46,50,53,55,66).

At atomistic level, we have analyzed the structure of water molecules around bridging Co-Hex between two DNAs when two DNAs strongly attract each other. As shown in Supplementary Figure S9 in Supplementary Material, bridging Co-Hex can induce the ordering of water molecules between adjacent phosphates in two DNAs, i.e. Co-Hex can induce the rotation of H_2O with O atoms pointing to Co-Hex and H atoms pointing to phosphates. Such configuration of bridging Co-Hex-induced ordering of water molecules between two helices could mediate an apparent DNA-DNA attraction, as suggested by Parsegian, Rau, Qiu and coworkers (13,19).

PMFs between A-RNAs at low, high and very high [Co-Hex]s

The PMFs between A-RNAs have been calculated at low (∼0.5 mM), high (∼5 mM) and very high (∼50 mM) [Co-Hex]'s, as shown in Figure 2d. At low (∼0.5 mM) [Co-Hex], in analogy to B-DNAs, the PMF between A-RNAs is repulsive and appears slightly stronger than that between B-DNAs. This may be attributed to the slightly higher charge density and thicker helix of A-RNAs (1). As [Co-Hex] is increased to ∼5 mM, the PMF between A-RNAs is still (weakly) repulsive with weaker strength than that at low [Co-Hex], which is distinctively in contrast to the strongly attractive PMF between B-DNAs. With the increase of [Co-Hex] to a very high value (∼50 mM), the PMF between A-RNAs becomes strongly attractive with free energy minimum of ∼-4.1k_BT at axis-axis separation of ∼27 Å. The predicted PMFs at different [Co-Hex]'s are in good accordance with the recent experiments on dsRNAs which have shown that dsRNAs resist condensation when [Co-Hex] <∼5 mM while could condense at very high [Co-Hex], relatively to the background Na^+ (30,31).

To understand the [Co-Hex]-dependent PMF between A-RNAs, we have analyzed the radial Co-Hex concentration distribution around A-RNAs (79), as shown in Figure 2e and f. For convenience, corresponding to the above termed 'external binding' with the radial distance range of [11–15 Å] (31), another binding mode with the radial distance range of <∼11 Å (∼helical radii of dsDNA and dsRNA) is termed as 'internal binding' (31). Overall, Co-

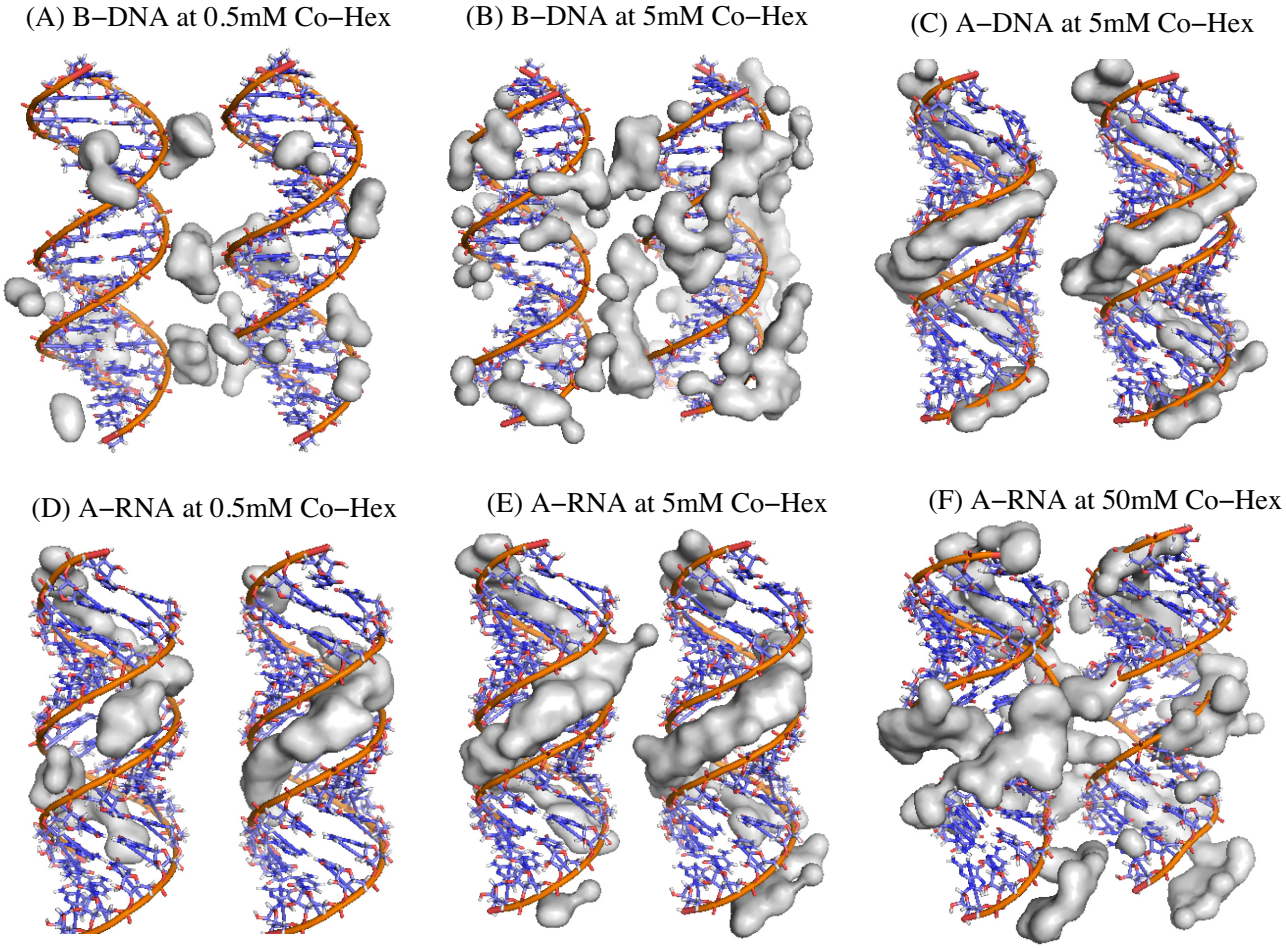

Figure 3. (**A** and **B**) The illustrations for the region of high Co-Hex ion charge density (larger than 0.02 $e/Å^3$) around two 16-bp B-DNAs in 0.5 mM (a) and 5 mM (b) Co-Hex solutions; (**C**) The illustration for the region of the high Co-Hex ion charge density (larger than 0.02 $e/Å^3$) around two 16-bp A-DNAs in 5 mM Co-Hex solutions. (**D**–**F**) The illustrations for the region of high Co-Hex charge density (larger than 0.02 $e/Å^3$) around two 16-bp A-RNAs in 0.5 mM (d), 5 mM (e) and 50 mM (f) Co-Hex solutions. Note that the buffers always contain 100 mM NaCl.

Hex ions begin to bind to A-RNA at radial distance $>\sim$2 Å, which is attributed to the accessible deep major groove of A-RNA. This is distinctly different from B-DNA. At low ($\sim$0.5 mM) [Co-Hex], Co-Hex ions exhibit 'internal binding' into the deep major groove within the radial distance of $<\sim$10 Å. As [Co-Hex] is increased to $\sim$5 mM, Co-Hex ions prefer to bind internally into the deep major groove around the radial distance of $\sim$8 Å, and Co-Hex binding distribution is extended to the radial distance range of $<\sim$12 Å. With the increase of [Co-Hex] to $\sim$50 mM, Co-Hex ions would still show preference to bind internally into the major groove around radial distance of 8–9 Å, while the apparent binding distribution is extended to the radial distance range of $<\sim$16 Å and the [Co-Hex] at $\sim$15 Å can nearly reach $\sim$0.3M. The concentration-dependent Co-Hex-binding distribution around A-RNA is understandable. At low [Co-Hex], Co-Hex would prefer to bind into the deep major groove with small radial distance where electric field is strongest (31), and as [Co-Hex] is increased, more Co-Hex ions become binding and begin to externally bind near outer surface of A-RNA after the deep/narrow major groove is fulfilled. Very high (e.g. $\sim$50 mM) [Co-Hex] would cause apparent 'external binding', and such apparent 'external binding' of Co-Hex can be shared by adjacent A-RNAs to cause an attractive PMF at very high [Co-Hex].

The 3-dimensional Co-Hex binding around two A-RNAs has been directly illustrated in Figure 3e and f. At low [Co-Hex], Co-Hex ions of high density are 'internal binding' in the deep and narrow major groove, and there is no visible ion-bridge between two A-RNA surfaces. At high ($\sim$5 mM) [Co-Hex], the abundant Co-Hex ions of high density reside in the major groove, and there is still no evident ion-bridge, which corresponds to the (weakly) repulsive PMF between A-RNAs. When [Co-Hex] is increased to $\sim$50 mM, many more Co-Hex ions become binding and the excess Co-Hex would bind externally at outer surface of A-RNAs, and the apparent ion-bridge between two A-RNAs is formed. Such ion-bridging configuration with Co-Hex-induced water ordering would be responsible for the strongly attractive PMF between A-RNAs at very high [Co-Hex] (46,50,53,55,66).

PMF is dependent on helical structure: dsRNA versus dsDNA

A-RNA versus B-DNA. Both A-RNAs and B-DNAs are highly (negatively) charged polymers, while the effective interaction between A-RNAs appears distinctly different from that between B-DNAs at high (∼5 mM) [Co-Hex], i.e. the PMF between B-DNAs is strongly attractive while that between A-RNAs is repulsive; see Figures 2a, d and 4a. As shown above, there are distinct differences between A-RNA and B-DNA in their topological structures. A-RNA has the deep/narrow major groove and the wide/shallow minor groove, as shown in Figure 3. Since there is strongest electric potential in the deep/narrow major groove of A-RNA, Co-Hex would prefer to bind deeply into major groove. Such 'internal binding' cannot contribute to the formation of ion-bridge between two A-RNAs and consequently the PMF is repulsive. Unlike A-RNA structure, B-DNA has the wide major groove and the narrow minor groove which are not deep compared with those of A-RNA, and Co-Hex ions would like to become 'external binding' near outer surface of B-DNA rather than 'internal binding' deeply into grooves. Such 'external binding' would help to form the apparent ion-bridge which could be shared by adjacent B-DNAs to result in an attractive PMF. When [Co-Hex] is increased to a very high value, the excess Co-Hex can also 'externally bind' to A-RNA since the deep/narrow major groove is fulfilled by more binding Co-Hex ions. Such 'external binding' induced by a very high [Co-Hex] can also promote the formation of ion-bridge and cause a strong attractive force between A-RNAs.

PMF between A-DNAs. To further confirm the above described effects of 'internal binding' and 'external binding', we have calculated and analyzed the PMF between two A-DNAs at 5 mM [Co-Hex]. As shown in Figure 4a, in analogy to A-RNA, the PMF between A-DNAs is repulsive at 5 mM [Co-Hex]. The detailed analysis on Co-Hex binding distribution also shows the 'internal binding' near the radial distance of ∼8 Å, which is similar to that of A-RNA; see Figure 4b and c. As illustrated in Figure 3c, such 'internal binding' is in deep major groove and resists the formation of ion-bridge, which is responsible for the (weakly) repulsive PMF between A-DNAs. It is noted here that despite the similarity in 'internal binding', the radial distribution of Co-Hex around A-DNA is slightly different from that around A-RNA: Co-Hex concentration around A-RNA is higher at radial distance of <∼5 Å, while lower at radial distance of ∼8 Å than that around A-DNA; see Figure 4b and c. Such difference comes from the difference in helical structures of A-RNA and A-DNA. Despite the similar A-form helical structure, as indicated in the experiments (81–83), the width of major groove of A-DNA is ∼2 Å narrower than that of A-RNA, which is also in accordance with our used structure parameters. The narrower major groove of A-DNA would cause Co-Hex ions to have more preference to bind in major groove and coordinate with adjacent phosphate strands at the radial distance of ∼8 Å, which has been observed in our MD simulations and illustrated in Figure 3c. The radial profiles of Co-Hex concentrations around A-form helices are in accordance with the previous experiments on Co-Hex binding to A-DNA, which showed that Co-Hex would bind to bases in major groove and to phosphates, either bridging across narrow major groove or residing between two adjacent intra-strand phosphates (84).

PMF between 'modified' A-RNAs. Since it is the 'internal binding' that resists the formation of ion-bridge and causes the repulsive PMF between A-RNAs, there would be an interesting question: If Co-Hex ions are prohibited to enter deeply into the major groove of A-RNAs, can A-RNAs attract each other? To answer the interesting question and further validate the above analysis, we have made the further calculations for the 'modified' A-RNAs (A-RNA' and A-RNA") at 5 mM [Co-Hex]. A-RNA' corresponds to the A-RNA with the bottom of the central 1/3 major groove fixed by a layer of water, and A-RNA" corresponds to the A-RNA with the bottom of the whole major groove fixed by a layer of water, as shown in Figure 5. Such treatment of fixing water at the bottom of deep major groove may effectively exclude the very deep binding of Co-Hex in major groove, and may possibly cause the 'external binding' and strong attractive force between the modified A-RNAs. Our calculations show that there are indeed apparently attractive forces between the 'modified' A-RNAs; see Figure 6a. The analyses on Co-Hex concentration distributions around the 'modified' A-RNAs also show that the treatment of excluding Co-Hex from the deep major groove promotes the 'external binding'. As shown in Figure 6b and c, when a layer of water is fixed at the bottom of major groove, the original 'internal binding' in the radial distance range of ∼2.5 Å to ∼12.5 Å would change into the binding in the radial distance range of ∼7 Å to ∼12.5 Å, and the 'external binding' near the radial distance of ∼13 Å. Furthermore, the direct illustration in Figure 5 shows that such treatment would definitely help to form the ion-bridge between two A-RNAs, which could cause the strong attractive PMF between the modified A-RNAs (46,50,53,55,66).

CONCLUSION

In this work, the atomistic MD simulations have been employed to calculate and analyze the potentials of mean force between A-RNAs, between B-DNAs, and between A-DNAs in Co-Hex solutions. The present work shows that though the nucleic acid helices have similar negative charge densities, the effective interactions between them are distinctively different. At high [Co-Hex], two B-DNAs strongly attract each other, while two A-RNAs and two A-DNAs repel each other. The present analysis shows that such significant difference between B-form and A-form helices is attributed to the ion-binding structure. For B-DNA, Co-Hex ions would become 'external binding' around phosphates and form the ion-bridge between two B-DNAs. But for A-RNA and A-DNA, due to the existence of deep major groove, Co-Hex would preferentially exhibit 'internal binding' into the major groove and consequently cannot form the ion-bridge between two A-form helices, causing the repulsive interaction between them. The effective interactions between A-RNAs can become strongly attractive when Co-Hex ions become 'external binding' to form the apparent ion-bridge, which can be realized by either increasing Co-

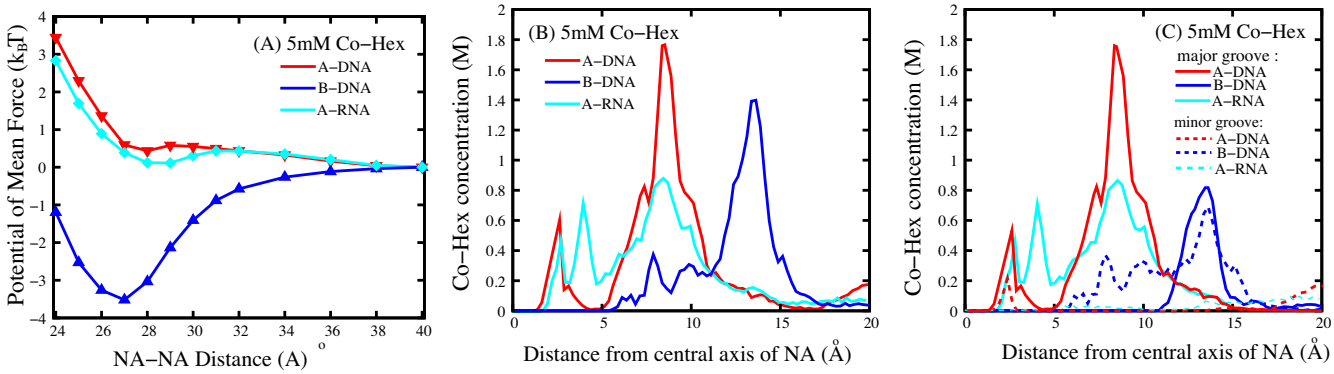

Figure 4. (**A**) The potentials of mean force between two 16-bp nucleic acid (B-DNA, A-RNA, and A-DNA) helices in 5 mM Co-Hex ion solution; (**B**) The Co-Hex distribution around the nucleic acid helices corresponding to panel a; (**C**) The Co-Hex distribution around the nucleic acid helices in (or over) major groove and minor groove corresponding to panels a and b. Note that the buffers always contain 100 mM NaCl.

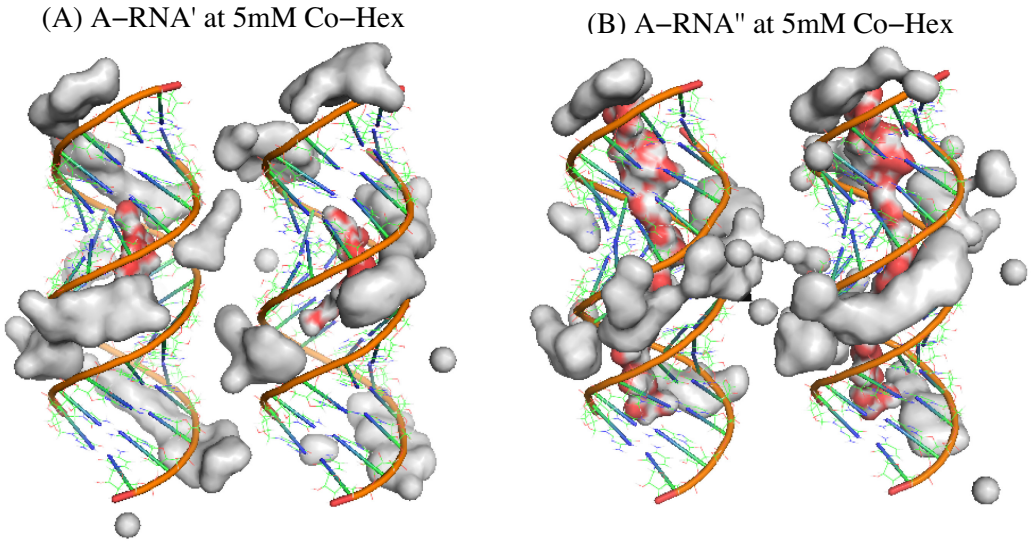

Figure 5. The illustrations for the spatially modified A-RNA (A-RNA' and A-RNA") and the region of the high Co-Hex charge density (larger than 0.02 $e/Å^3$) in 5 mM Co-Hex solution around two 16-bp A-RNA's and around two 16-bp A-RNA's. The A-RNA' denotes the A-RNA with the bottom of the central 1/3 major groove fixed with a layer of water, whereas the A-RNA" denotes the A-RNA with the bottom of the entire major groove fixed with a layer of water. The red-gray chains in deep major grooves illustrate the fixed water molecules. Note that the buffers always contain 100 mM NaCl.

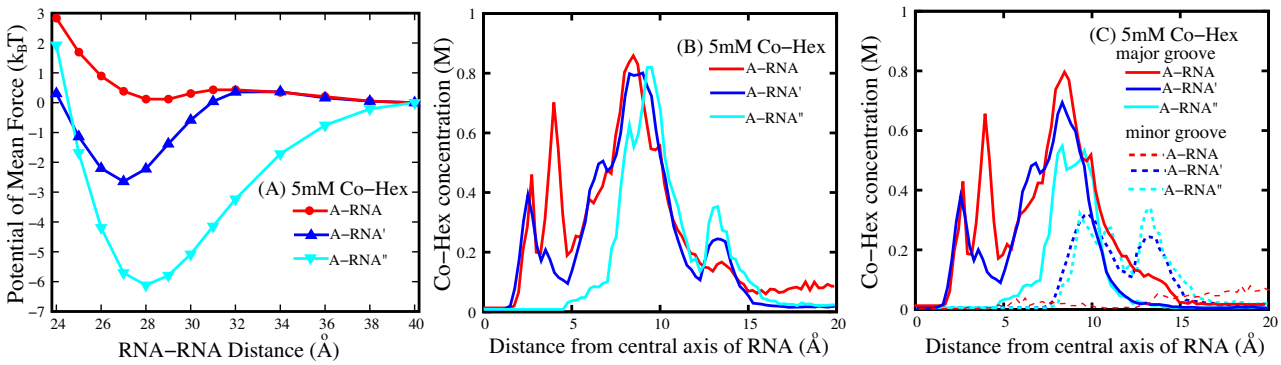

Figure 6. (**A**) The potentials of mean force between two 16-bp A-RNAs, between two 16-bp A-RNA's, and between 16-bp A-RNA"s in 5 mM Co-Hex ion solution; (**B**) The Co-Hex distributions around the A-RNA, A-RNA', and A-RNA" corresponding to panels a and b; (**C**) The Co-Hex distributions around the A-RNA, A-RNA', and A-RNA" in (or over) major groove and minor groove corresponding to panels a and b. The A-RNA' denotes the A-RNA with the bottom of the central 1/3 major groove fixed with a layer of water, whereas the A-RNA" denotes the A-RNA with the bottom of the entire major groove fixed with a layer of water. Note that the buffers always contain 100 mM NaCl.

Hex to a very high concentration or fixing a layer of water at the bottom of the deep major groove.

Overall, our results are in accordance with the experimental findings (17,30,31,77). First, our calculations show that the PMF between A-RNAs is weakly repulsive while that between B-DNAs is strongly attractive at ∼5 mM Co-Hex, which is in good agreement with the recent experiments (30,31). Second, Parsegian, Rau and coworkers combined single-molecule magnetic tweezers with osmotic stress on DNA assembly in various salt solutions. Their direct measurement of the free energy for DNA aggregates in Co-Hex solution is ∼-0.21 k_BT/bp (17), a value close to ours of ∼−3.5k_BT for 16-bp DNAs, and the separation of ∼27 Å at the lowest free energy for ∼5 mM Co-Hex from our MD simulations is also close to the experimental equilibrium spacing ∼28 Å of DNA aggregate (15,17). Third, the calculated osmotic pressures with assuming additivity of PMF are very close to the corresponding experimental measurements (15,16).

Kornyshev and Leikin have successfully developed their electrostatic zipper model to explain why A-RNAs resist condensation while B-DNAs would become condensed, and such distinctive behaviors were proposed to be attributed to the different widths of the major grooves of different helices (42). However, the model has also involved some important simplifications such as assuming the uniform distribution of ions in grooves and ignoring ion size and 3-dimensional ion-accessible geometry of different helices. The present all-atom MD simulations with explicit helical structures, ions and water molecules, show that the 3-dimensional topology of different helices can play an important role in modulating PMF between two helices. Specifically, the attractive PMF between B-DNA at ∼5 mM Co-Hex is accompanied with the external binding of Co-Hex above major groove at radial distance of ∼13 Å, while the non-attractive PMF between A-RNAs at ∼5 mM Co-Hex is accompanied with the internal binding of Co-Hex at radial distance of ∼8–9 Å in major groove.

The present work has also involved some assumptions and simplifications. First, all the dsRNAs and dsDNAs have been approximately treated as rigid bodies and thus the stability and flexibility of ds helices have been ignored. Since all the nucleic acid helices are in solutions of 100 mM NaCl, the helices would have high stability to keep its helical structure rather than become denatured (85,86). Although nucleic acid helices are flexible in ionic solutions, the ignorance of helix flexibility can be a reasonable approximation due to the high persistence length (45–60 nm) (81,82) and strong stretching modulus (>∼500 pN) (74,87,88) of dsDNA and dsRNA. Second, we have made the calculations for A-DNAs without considering the likely dependence of A-DNA structure on ionic condition (1). It is a reasonable simplified treatment since we only use A-DNA as a structure model to further examine the mechanism. Thirdly, the extensive relevant experiments have used the 25-bp dsRNA and dsDNA helices (30,31), while 16-bp dsRNAs and dsDNAs have been employed in the work for saving the computational time. Such simplification would not affect the conclusions since the experiments have shown that 16-bp dsDNAs have the similar Co-Hex-dependent condensation behavior (30). Fourthly, the related experiments involve different background Na^+ concentrations of 100 mM and 20 mM with different experiment techniques (30,31), while the present work only considers the solutions containing 100 mM Na^+. Such simplification should not qualitatively affect our conclusions since the experiments with different background Na^+ concentrations have shown the qualitatively similar results (30,31). The effect of competition between Co-Hex and background Na^+ on the effective nucleic acid helix-helix interaction may deserve to be studied separately.

Furthermore, in the present work, we only consider the parallel configuration of two helices with all the atoms restrained in y and z directions, and the helices cannot rotate around any of the x, y and z axes. In fact, such parallel configuration would be the most favorable one for large separation between two helices (89), while may become unfavorable for the closely packaging of two helices, due to the strong electrostatic repulsion (28,29). In realistic 3D space, the axes of two helices at small separation can rotate by a small angle to form a typical X-shaped structure (90,91) with several possible packaging modes for different helical structures (90,91). Such tight non-parallel helix-helix configuration may be important for the packaging of some RNAs such as the P4-P6 domain of the Tetrahymena thermophila intron (92).

Finally, the present work only involves the system of two helices while the related experiments generally involved multiple helices. The previous studies have shown that the multi-body effect may slightly affect the multivalent-mediated helix-helix attraction and consequently may slightly affect the comparisons between our predictions and experiments on the interaction strength and axis-axis separation (28). The strict and extensive exploration for multi-body PMF between helices at atomistic level is deserved to be studied separately.

Nevertheless, the present work has provided the direct calculations on the PMFs between A-RNAs, between B-DNAs and between A-DNAs, and has directly illustrated the microscopic mechanisms for the different PMFs between double-stranded nucleic acids with different helical structures.

SUPPLEMENTARY DATA

Supplementary Data are available at NAR Online.

ACKNOWLEDGEMENTS

We are grateful to Profs. Shi-Jie Chen, Haiping Fang and Wenbing Zhang for valuable discussions, and Chang Shu for facility assistance.

FUNDING

National Key Scientific Program (973)—Nanoscience and Nanotechnology [2011CB933600]; National Science Foundation of China [11074191, 11175132 and 11374234]; Program for New Century Excellent Talents [NCET 08-0408]. One of us (Y.Y. Wu) also thanks the financial support from the interdisciplinary and postgraduate programs under the Fundamental Research Funds for the Central Universities. Funding for open access charge: The National Science Foundation of China.

Conflict of interest statement. None declared.

REFERENCES

1. Bloomfield,V.A., Crothers,D.M. and Tinoco,I. Jr (2000) *Nucleic Acids: Structures, Properties, and Functions*. University Science Books, Sausalito. CA.
2. Bloomfield,V.A. (1997) DNA Condensation by multivalent cations. *Biopolymers*, **44**, 269–282.
3. Chen,S.J. (2008) RNA folding: conformational statistics, folding kinetics, and ion electrostatics. *Annu. Rev. Biophys.*, **37**, 197–214.
4. Woodson,S.A. (2010) Compact intermediates in RNA folding. *Annu. Rev. Biophys.*, **39**, 61–77.
5. Wong,G.C. and Pollack,L. (2010) Electrostatics of strongly charged biological polymers: ion-mediated interactions and self-organization in nucleic acids and proteins. *Annu. Rev. Phys. Chem.*, **61**, 171–189.
6. Auffinger,P., Grover,N. and Westhof,E. (2011) Metal ion binding to RNA[J]. *Met. Ions Life Sci.*, **9**, 1–35.
7. Draper,D.E. (2013) Folding of RNA tertiary structure: linkages between backbone phosphates, ions, and water. *Biopolymers*, **99**, 1105–1113.
8. Lipfert,J., Doniach,S., Das,R. and Herschlag,D. (2014) Understanding nucleic acid-ion interactions. *Annu. Rev. Biochem.*, **83**, 813–841.
9. Koculi,E., Hyeon,C., Thirumalai,D. and Woodson,S.A. (2007) Charge density of divalent metal cations determines RNA stability. *J. Am. Chem. Soc.*, **129**, 2676–2682.
10. Tan,Z.J. and Chen,S.J. (2011) Importance of diffuse metal ion binding to RNA. *Met. Ions Life Sci.*, **9**, 101–124.
11. Williams,L.D. and Maher,L.J. III (2000) Electrostatic mechanisms of DNA deformation. *Annu. Rev. Biophys. Biomol. Struct.*, **29**, 497–521.
12. Widom,J. and Baldwin,R.L. (1980) Cation-induced toroidal condensation of DNA studies with $Co^{3+}(NH_3)_6$. *J. Mol. Biol.*, **144**, 431–453.
13. DeRouchey,J., Parsegian,V.A. and Rau,D.C. (2010) Cation charge dependence of the forces driving DNA assembly. *Biophys. J.*, **99**, 2608–2615.
14. Korolev,N., Berezhnoy,N.V., Eom,K.D., Tam,J.P. and Nordenskiöld,L. (2012) A universal description for the experimental behavior of salt-(in)dependent oligocation-induced DNA condensation. *Nucleic Acids Res.*, **40**, 2808–2821.
15. Rau,D.C. and Parsegian,V.A. (1992) Direct measurement of temperature-dependent solvation forces between DNA double helices. *Biophys. J.*, **61**, 260–271.
16. Rau,D.C. and Parsegian,V.A. (1992) Direct measurement of the intermolecular forces between counterion-condensed DNA double helices. Evidence for long range attractive hydration forces. *Biophys. J.*, **61**, 246–259.
17. Todd,B.A., Parsegian,V.A., Shirahata,A., Thomas,T.J. and Rau,D.C. (2008) Attractive forces between cation condensed DNA double helices. *Biophys. J.*, **94**, 4775–4782.
18. Qiu,X., Andresen,K., Kwok,L.W., Lamb,J.S., Park,H.Y. and Pollack,L. (2007) Inter-DNA Attraction Mediated by Divalent Counterions. *Phys. Rev. Lett.*, **99**, 038104.
19. Qiu,X., Parsegian,V.A. and Rau,D.C. (2010) Divalent Counterion-induced condensation of triple-strand DNA. *Proc. Natl. Acad. Sci. USA*, **107**, 21482–21486.
20. Butler,J.C., Angelini,T., Tang,J.X. and Wong,G.C. (2003) Ion multivalence and like-charge polyelectrolyte attraction. *Phys. Rev. Lett.*, **91**, 028301.
21. Wu,J.Z., Bratko,D. and Prausnitz,J.M. (1998) Interaction between like-charged colloidal spheres in electrolyte solutions. *Proc. Natl. Acad. Sci. USA*, **95**, 15169–15172.
22. Solis,F.J. and Olvera de la Cruz,M. (2000) Collapse of flexible polyelectrolytes in multivalent salt solutions. *J. Chem. Phys.*, **112**, 2030–2035.
23. Angelini,T.E., Liang,H., Wriggers,W. and Wong,G.C. (2003) Like-charge attraction between polyelectrolytes induced by counterion charge density waves. *Proc. Natl. Acad. Sci. USA*, **100**, 8634–8637.
24. Tang,J.X., Janmey,P.A., Lyubartsev,A. and Nordenskiöld,L. (2002) Metal ion-induced lateral aggregation of filamentous viruses fd and m13. *Biophys. J.*, **83**, 566–581.
25. Wen,Q. and Tang,J.X. (2006) Temperature effects on threshold counterion concentration to induce aggregation of fd virus. *Phys. Rev. Lett.*, **97**, 048101.
26. Bai,Y., Das,R., Millett,I.S., Herschlag,D. and Doniach,S. (2005) Probing counterion modulated repulsion and attraction between nucleic acid duplexes in solution. *Proc. Natl. Acad. Sci. USA*, **102**, 1035–1040.
27. Bai,Y., Chu,V.B., Lipfert,J., Pande,V.S., Herschlag,D. and Doniach,S. (2008) Critical assessment of nucleic acid electrostatics via experimental and computational investigation of an unfolded state ensemble. *J. Am. Chem. Soc.*, **130**, 12334–12341.
28. Tan,Z.J. and Chen,S.J. (2006) Electrostatic free energy landscapes for nucleic acid helix assembly. *Nucleic Acids Res.*, **34**, 6629–6639.
29. Tan,Z.J. and Chen,S.J. (2012) Ion-mediated RNA structural collapse: effect of spatial confinement. *Biophys. J.*, **103**, 827–836.
30. Li,L., Pabit,S.A., Meisburger,S.P. and Pollack,L. (2011) Double-stranded RNA resists condensation. *Phys. Rev. Lett.*, **106**, 108101.
31. Tolokh,I.S., Pabit,S.A., Katz,A.M., Chen,Y., Drozdetski,A., Baker,N., Pollack,L. and Onufriev,A.V. (2014) Why double-stranded RNA resists condensation. *Nucleic Acids Res.*, **42**, 10823–10831.
32. Pabit,S.A., Qiu,X., Lamb,J.S., Li,L., Meisburger,S.P. and Pollack,L. (2009) Both helix topology and counterion distribution contribute to the more effective charge screening in dsRNA compared with dsDNA. *Nucleic Acids Res.*, **37**, 3887–3896.
33. Manning,G.S. (1978) The Molecular theory of polyelectrolyte solutions with applications to the electrostatic properties of polynucleotides. *Q. Rev. Biophys.*, **11**, 179–246.
34. Ray,J. and Manning,G.S. (1994) An attractive force between two rodlike polyions mediated by the sharing of condensed counterions. *Langmuir.*, **10**, 2450–2461.
35. Baker,N.A., Sept,D., Joseph,S., Holst,M.J. and McCammon,J.A. (2001) Electrostatics of nanosystems: Application to microtubules and the ribosome. *Proc. Natl. Acad. Sci. USA*, **98**, 10037–10041.
36. Boschitsch,A.H., Fenley,M.O. and Zhou,H. (2002) Fast boundary element method for the linear Poisson-Boltzmann equation. *J. Phys. Chem. B*, **106**, 2741–2754.
37. Baker,N.A. (2004) Poisson–Boltzmann methods for biomolecular electrostatics. *Method. Enzymol.*, **383**, 94–118.
38. Lu,B., Cheng,X., Huang,J. and McCammon,J.A. (2010) AFMPB: an adaptive fast multipole Poisson–Boltzmann solver for calculating electrostatics in biomolecular systems. *Comput. Phys. Commun.*, **181**, 1150–1160.
39. Chen,D., Chen,Z., Chen,C., Geng,W. and Wei,G.W. (2011) MIBPB: a software package for electrostatic analysis. *J. Comput. Chem.*, **32**, 756–770.
40. Wei,G.W., Zheng,Q., Chen,Z. and Xia,K. (2012) Variational multiscale models for charge transport. *SIAM Rev.*, **54**, 699–754.
41. Ovanesyan,Z., Medasani,B., Fenley,M.O., Guerrero-García,G.I., Olvera de la Cruz,M. and Marucho,M. (2014) Excluded volume and ion-ion correlation effects on the ionic atmosphere around B-DNA: Theory, simulations, and experiments. *J. Chem. Phys.*, **141**, 225103.
42. Kornyshev,A.A. and Leikin,S. (2013) Helical structure determines different susceptibilities of dsDNA, dsRNA, and tsDNA to counterion-induced condensation. *Biophys. J.*, **104**, 2031–2041.
43. Kornyshev,A.A. and Leikin,S. (1999) Electrostatic zipper motif for DNA aggregation. *Phys. Rev. Lett.*, **82**, 4138–4141.
44. Tan,Z.J. and Chen,S.J. (2005) Electrostatic correlations and fluctuations for ion binding to a finite length polyelectrolyte. *J. Chem. Phys.*, **122**, 044903.
45. Tan,Z.J. and Chen,S.J. (2010) Predicting ion binding properties for RNA tertiary structures. *Biophys. J.*, **99**, 1565–1576.
46. Tan,Z.J. and Chen,S.J. (2006) Ion-mediated nucleic acid helix-helix Interactions. *Biophys. J.*, **91**, 518–536.
47. Tan,Z.J. and Chen,S.J. (2011) Salt contribution to RNA tertiary structure folding stability. *Biophys. J.*, **101**, 176–187.
48. Lyubartsev,A.P. and Nordenskiold,L. (1995) Monte Carlo simulation study of ion distribution and osmotic pressure in hexagonally oriented DNA. *J. Phys. Chem.*, **99**, 10373–10382.
49. Allahyarov,E., Gompper,G. and Löwen,H. (2004) Attraction between DNA molecules mediated by multivalent ions. *Phys. Rev. E*, **69**, 041904.

50. Wang,F.H., Wu,Y.Y. and Tan,Z.J. (2013) Salt contribution to the flexibility of single-stranded nucleic acid of finite length. *Biopolymers*, **99**, 370–381.
51. Shi,Y.Z., Wang,F.H., Wu,Y.Y. and Tan,Z.J. (2014) A coarse-grained model with implicit salt for RNAs: predicting 3D structure, stability and salt effect. *J. Chem. Phys.*, **141**, 105102.
52. Feig,M. and Pettitt,B.M. (1998) Structural equilibrium of DNA represented with different force fields. *Biophys. J.*, **75**, 134–149.
53. Luan,B. and Aksimentiev,A. (2008) DNA attraction in monovalent and divalent electrolytes. *J. Am. Chem. Soc.*, **130**, 15754–15755.
54. Maffeo,C., Luan,B. and Aksimentiev,A. (2012) End-to-end attraction of duplex DNA. *Nucleic Acids Res.*, **40**, 3812–3821.
55. Dai,L., Mu,Y., Nordenskiöld,L. and van der Maarel,J.R. (2008) Molecular dynamics simulation of multivalent-ion mediated attraction between DNA molecules. *Phys. Rev. Lett.*, **100**, 118301.
56. Anandakrishnan,R., Drozdetski,A., Walker,R.C. and Onufriev,A.V. (2015) Speed of conformational change: comparing explicit and implicit solvent molecular dynamics simulations. *Biophys. J.*, **108**, 1153–1164.
57. Anandakrishnan,R., Aguilar,B. and Onufriev,A.V. (2012). H++ 3.0: automating pK prediction and the preparation of biomolecular structures for atomistic molecular modeling and simulations. *Nucleic Acids Res.*, **40**, W537–W541.
58. Yu,T., Wang,X.Q., Sang,J.P., Pan,C.X., Zou,X.W., Chen,T.Y. and Zou,X. (2012). Influences of mutations on the electrostatic binding free energies of chloride ions in Escherichia coli ClC. *J. Phys. Chem. B*, **116**, 6431–6438.
59. Wang,X.Q., Yu,T., Sang,J.P., Zou,X.W., Chen,T.Y., Bolser,D. and Zou,X. (2010). A three-state multi-ion kinetic model for conduction properties of ClC-0 chloride channel. *Biophys. J.*, **99**, 464–471.
60. Zhang,Y., Zhang,J. and Wang,W. (2011) Atomistic analysis of pseudoknotted RNA unfolding. *J. Am. Chem. Soc.*, **133**, 6882–6885.
61. Li,W., Nordenskiöld,L., Zhou,R. and Mu,Y. (2014) Conformation-dependent DNA attraction. *Nanoscale*, **6**, 7085–7092.
62. Gong,Z., Zhao,Y., Chen,C, Duan,Y. and Xiao,Y. (2014) Insights into ligand binding to PreQ1 riboswitch aptamer from molecular dynamics simulations. *PloS One*, **9**, e92247.
63. Auffinger,P. and Westhof,E. (1998) Simulations of the molecular dynamics of nucleic acids. *Curr. Opin. Struc. Boil.*, **8**, 227–236.
64. Pérez,A., Marchán,I., Svozil,D., Sponer,J., Cheatham,T.E. III, Laughton,C.A. and Orozco,M. (2007) Refinement of the AMBER force field for nucleic acids: improving the description of α/γ conformers. *Biophys. J.*, **92**, 3817–3829.
65. Van Der Spoel,D., Lindahl,E., Hess,B., Groenhof,G., Mark,A.E. and Berendsen,H.J. (2005) GROMACS: fast, flexible, and free. *J. Comput. Chem.*, **26**, 1701–1718.
66. Wu,Y.Y., Wang,F.H. and Tan,Z.J. (2013) Calculating potential of mean force between like-charged nanoparticles: a comprehensive study on salt effects. *Phys. Lett. A*, **377**, 1911–1919.
67. Braunlin,W.H., Anderson,C.F. and Record,M.T. Jr (1987) Competitive interactions of cobalt (3+) hexamine and sodium with helical B-DNA probed by cobalt-59 and sodium-23 NMR. *Biochemistry*, **26**, 7724–7731.
68. Cheatham,T.E. and Kollman,P.A. (1997) Insight into the stabilization of A-DNA by specific ion association: spontaneous B-DNA to A-DNA transitions observed in molecular dynamics simulations of d[ACCCGCGGGT]$_2$ in the presence of hexaamminecobalt (III). *Structure*, **5**, 1297–1311.
69. Marques,H.M. and Brown,K.L. (2002) Molecular mechanics and molecular dynamics simulations of porphyrins, metalloporphyrins, heme proteins and cobalt corrinoids. *Coord. Chem. Rev.*, **225**, 123–158.
70. Galindo-Murillo,R. and Cheatham,T.E. (2014) DNA binding dynamics and energetics of cobalt, nickel, and copper metallopeptides. *Chem. Med. Chem.*, **9**, 1252–1259.
71. Hess,B., Kutzner,C., Van Der Spoel,D. and Lindahl,E. (2008) GROMACS 4: algorithms for highly efficient, load-balanced, and scalable molecular simulation. *J. Chem. Theory Comput.*, **4**, 435–447.
72. Essmann,U., Perera,L., Berkowitz,M.L., Darden,T., Lee,H. and Pedersen,L.G. (1995) A smooth particle mesh Ewald method. *J. Chem. Phys.*, **103**, 8577–8593.
73. Hess,B., Bekker,H., Berendsen,H.J. and Fraaije,J.G. (1997) LINCS: a linear constraint solver for molecular simulations. *J. Comput. Chem.*, **18**, 1463–1472.
74. Wu,Y.Y., Bao,L., Zhang,X. and Tan,Z.J. (2015) Flexibility of short DNAs with finite-length effect: from base pairs to tens of base pairs. *J. Chem. Phys.*, **142**, 125103.
75. Kästner,J. and Thiel,W. (2005) Bridging the gap between thermodynamic integration and umbrella sampling provides a novel analysis method: 'Umbrella integration'. *J. Chem. Phys.*, **123**, 144104.
76. Qiu,X., Giannini,J., Howell,S.C., Xia,Q., Ke,F. and Andresen,K. (2013) Ion competition in condensed DNA arrays in the attractive regime. *Biophys. J.*, **105**, 984–992.
77. Qiu,X., Rau,D.C., Parsegian,V.A., Fang,L.T., Knobler,C.M. and Gelbart,W.M. (2011) Salt-dependent DNA-DNA spacings in intact bacteriophage λ reflect relative importance of DNA self-repulsion and bending energies. *Phys. Rev. Lett.*, **106**, 028102.
78. He,Z. and Chen,S.J. (2013) Quantifying Coulombic and solvent polarization-mediated forces between DNA helices. *J. Phys. Chem. B*, **117**, 7221–7227.
79. Kirmizialtin,S., Silalahi,A.R., Elber,R. and Fenley,M.O. (2012) The ionic atmosphere around A-RNA: Poisson-Boltzmann and molecular dynamics simulations. *Biophys. J.*, **102**, 829–838.
80. Alsharif,S.A., Chen,L.Y., Tlahuice-Flores,A., Whetten,R.L. and Yacaman,M.J. (2014) Interaction between functionalized gold nanoparticles in physiological saline. *Phys. Chem. Chem. Phys.*, **16**, 3909–3913.
81. McKee,T. and McKee,J.R. (2009) *Biochemistry: the molecular basis of life*. Oxford University Press, NY.
82. Weeks,K.M. and Crothers,D.M. (1993) Major groove accessibility of RNA. *Science*, **261**, 1574–1574.
83. Shakked,Z., Rabinovich,D., Cruse,W.B.T., Egert,E., Kennard,O., Sala,G.S., Salisbury,A. and Viswamitra,M.A. (1981) Crystalline A-DNA: the X-ray analysis of the fragment d (GGTATACC). *Proc. R. Soc. London B*, **213**, 479–487.
84. Gao,Y.G., Robinson,H., van Boom,J.H. and Wang,A.H. (1995) Influence of counter-ions on the crystal structures of DNA decamers: binding of $[Co(NH_3)_6]^{3+}$ and Ba^{2+} to A-DNA. *Biophys. J.*, **69**, 559–568.
85. Tan,Z.J. and Chen,S.J. (2007) RNA helix stability in mixed Na^+/Mg^{2+} solution. *Biophys. J.*, **92**, 3615–3632.
86. Tan,Z.J. and Chen,S.J. (2006) Nucleic acid helix stability: effects of salt concentration, cation valence and size, and chain length. *Biophys. J.*, **90**, 1175–1190.
87. Lipfert,J., Skinner,G.M., Keegstra,J.M., Hensgens,T., Jager,T., Dulin,D., Köber,M., Yu,Z., Donkers,S.P., Chou,F.C., Das,R. *et al.* (2014) Double-stranded RNA under force and torque: similarities to and striking differences from double-stranded DNA. *Proc. Natl. Acad. Sci. USA.*, **111**, 15408–15413.
88. Herrero-Galán,E., Fuentes-Perez,M.E., Carrasco,C., Valpuestam,J.M., Carrascosam,J.L., Moreno-Herrero,F. and Arias-Gonzalez,J.R. (2013) Mechanical identities of RNA and DNA double helices unveiled at the single-molecule level. *J. Am. Chem. Soc.*, **135**, 122–131.
89. Kornyshev,A.A. and Leikin,S. (2000) Electrostatic interaction between long, rigid helical macromolecules aat ll interaxial angles. *Phys. Rev. E*, **62**, 2576–2596.
90. Murthy,V.L. and Rose,G.D. (2000) Is counterion delocalization responsible for collapse in RNA folding? *Biochemistry*, **39**, 14365–14370.
91. Várnai,P. and Timsit,Y. (2010) Differential stability of DNA crossovers in solution mediated by divalent cations. *Nucleic Acids Res.*, **38**, 4163–4172.
92. Cate,J.H., Gooding,A. R, Podell,E., Zhou,K., Golden,B.L., Kundrot,C.E., Cech,T.R. and Doudna,J.A. (1996) Crystal structure of a group I ribozyme domain: principles of RNA packing. *Science*, **273**, 1678–1685.